

# Equivalent System Model and Equalization of Differential Impulse Radio UWB Systems

Klaus Witrisal, *Member, IEEE*, Geert Leus, *Member, IEEE*, Marco Pausini, *Student Member, IEEE*, and Christoph Krall, *Student Member, IEEE*

**Abstract**—A discrete-time equivalent system model is derived for differential and transmitted reference (TR) ultra-wideband (UWB) impulse radio (IR) systems, operating under heavy intersymbol-interference (ISI) caused by multipath propagation. In the systems discussed, data is transmitted using differential modulation on a frame-level, i.e., among UWB pulses. Multiple pulses (frames) are used to convey a single bit. Time hopping and amplitude codes are applied for multi user communications, employing a receiver front-end that consists of a bank of pulse-pair correlators.

It is shown that these UWB systems are accurately modeled by second-order discrete-time Volterra systems. This proposed nonlinear equivalent system model is the basis for developing optimal and suboptimal receivers for differential UWB communications systems under ISI. As an example, we describe a maximum likelihood sequence detector with decision feedback, to be applied at the output of the receiver front-end sampled at symbol rate, and an adaptive inverse modeling equalizer. Both methods significantly increase the robustness in presence of multipath interference at tractable complexity.

**Index Terms**—Differential receivers, equalization, impulse radio (IR), transmitted reference, ultra-wideband (UWB) communications, Volterra systems.

## I. INTRODUCTION

IN autocorrelation receiver (AcR) front-ends for impulse radio (IR) ultra-wideband (UWB) communications systems, the received signal consisting of a train of pulses is delayed and correlated with itself. The basic idea is to use the delayed signal as a template in the demodulation block, without requiring any kind of channel estimation. Thus, one pulse is used to “sound” the channel and another one is used to convey data. Data can be applied, for instance, by differentially modulating the polarity of the “data” pulse with respect to the “reference” pulse. The delay line in an AcR front-end, or “pulse-pair” correlator, is matched to the lag between the reference and the data pulses. The overall system is often called a transmitted reference (TR) AcR [1]–[13].

Manuscript received March 31, 2004; revised January 22, 2005 and March 20, 2005. The work of G. Leus was supported in part by NWO-STW under the VICI Program (DTC.5893). The work of M. Pausini was supported in part by the Dutch Ministry of Economic Affairs/Ministry of Education Freeband-Impulse Project *Airlink*. This paper was presented in part at the IEEE Global Telecommunications Conference (GLOBECOM), Dallas, TX, November/December 2004.

K. Witrisal and C. Krall are with the Signal Processing and Speech Communication Laboratory and the Christian Doppler Laboratory for Nonlinear Signal Processing, Graz University of Technology, A-8010 Graz, Austria (e-mail: Witrisal@tugraz.at; Christoph.Krall@tugraz.at).

G. Leus and M. Pausini are with the Circuits and Systems Group and the Wireless and Mobile Communications Group, Delft University of Technology, NL-2628 CD Delft, The Netherlands (e-mail: Leus@cas.et.tudelft.nl; M.Pausini@ewi.tudelft.nl).

Digital Object Identifier 10.1109/JSAC.2005.853876

AcRs have the big advantage of capturing energy from all multipath components at low implementation complexity, compared with coherent receivers. Unfortunately the reference pulse is corrupted by noise and interference, which is an inherent disadvantage. If the data rate of such systems is increased, interference among multiple pulses becomes one of the most fundamental deteriorating effects, due to the multipath propagation. This effect is termed interframe-interference (IFI), if interference between multiple pulses of one data symbol is referred to, and intersymbol-interference (ISI) for the interference among consecutive data symbols. The characterization, modeling, and suppression of IFI and ISI is still a young topic of research. A few important basic results are found, e.g., in [2], [4], and [14]. However, most of them are limited to rather simple cases, for example considering IFI among a pair of reference and data pulses only [2], [4]. A more sophisticated model has been presented in [12], where both IFI and ISI are taken into consideration. Based on this work, linear weighting of an oversampled AcR output is suggested in [13] to improve the receiver performance. Most other previous works assume pulse spacings sufficiently long such that IFI is completely avoided, which ultimately limits the transmission rates [5]–[11].

In this paper, we derive an equivalent system model for AcR-based UWB systems, describing the IFI and ISI in a multipath channel. That is, high-rate differential transmission schemes are studied. The system model accurately relates the transmitted data bits  $\{d_i\}$  to the test statistics at the decision device  $\hat{z}[i]$ . A nonlinear second-order Volterra model [15] is found to describe the data dependency, whereby the nonlinearity is caused by the multiplication in the pulse-pair correlators. The data model can be written as

$$\hat{z}[i] = h_0 + \sum_{n=-\eta}^1 h_{1,n} d_{i+n} + \sum_{n=-\eta}^1 \sum_{m=n+1}^1 h_{2,n,m} d_{i+n} d_{i+m} + z_\nu[i]. \quad (1)$$

Besides a linear finite impulse response (FIR) component specified by the coefficients  $h_{1,n}$ , it comprises an additive bias term  $h_0$  and product terms of the transmitted data symbols, weighted by the second-order coefficients  $h_{2,n,m}$ . The memory depth is expressed by  $\eta$ , which is determined by the ratio of the maximum channel excess delay and the symbol duration. Additive noise samples are denoted by  $z_\nu[i]$ , whose second-order moments are studied in this paper. We will demonstrate the suitability of this model for the differential UWB scheme described in [14]. This scheme achieves higher efficiency and potentially

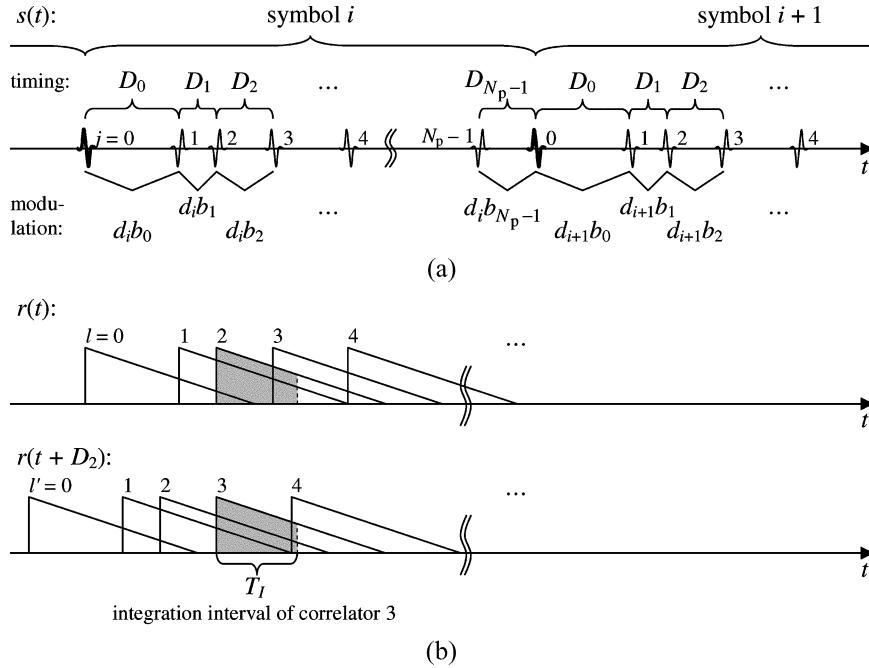


Fig. 1. Illustration of the (a) transmitted and (b) received signals in the studied differential UWB system. In (b), the correlation lag  $D_2$  and integration interval  $T_I$  is shown for the correlation of the reference pulse  $l = 2$  and the data pulse  $l' = 3$ .

supports higher data rates by differentially modulating each pulse with respect to the previous one—so each pulse is used as a reference *and* as a data pulse.

The derived equivalent system model is a powerful tool for developing optimal and suboptimal detection algorithms (equalizers) for high-rate differential UWB schemes suffering from ISI. Its structure holds under various modifications and system imperfections, like fractional sampling, separate processing of multiple AcR channels, mismatching transmitter and receiver parameters, synchronization and delay errors, and others. It can be extended to a multiuser model. It is also useful in the performance evaluation and optimization under ISI conditions, as demonstrated in this paper and in [16].

As an example for the model's applicability, we demonstrate the equalization of the differential IR system, using a maximum-likelihood (ML) sequence detector with decision feedback and an adaptive inverse modeling approach. These algorithms are implemented in the back-end of the receiver, processing the output signal of the analog front-end, which is uniformly sampled at the symbol rate. Significantly increased data rates (at a given channel delay spread) or, equivalently, higher robustness against multipath interference (at fixed data rates) are potentially obtainable, if accurate synchronization and channel estimation could be achieved.

We do not investigate the problems of channel estimation and synchronization in this paper, which are crucial for practical implementations. However, through the use of the proposed equivalent system model, we are able to convert the channel impulse response into a set of “low-rate” channel parameters, which can be estimated from the front-end output  $\hat{z}[i]$ . Similarly, the synchronization problem is simplified because shifted from the pulse level (subnanosecond scale) to the symbol level (phase synchronization of a symbol clock). Most critically, the performance of the investigated schemes will be affected by the delay-line accu-

racy, comparable to the required accuracy of the local oscillator in a conventional bandpass system. This is considered to be the major implementation challenge for UWB AcRs.

This paper is organized as follows. The differential receiver concept and its signal model are presented in Section II. In Section III, the equivalent system model is derived, first, neglecting noise, which is then introduced in Section IV. Validation results and their discussion can be found in Section V, along with performance results of a conventional threshold detector. In Section VI, we demonstrate the equalization of the proposed receiver, followed by conclusions in Section VII.

## II. MATHEMATICAL MODELING

### A. Transmitted Signal

In this section, the signal model is given for the differential IR-UWB schemes under investigation. Each data symbol  $\{d_i\} \in \mathbb{B} = \{-1, +1\}$ ,  $i$  being the symbol index, is transmitted via  $N_p$  consecutive pulses. This data symbol sequence is spread by a pseudorandom amplitude code sequence  $\{b_j\} \in \mathbb{B}$ , where  $j = 0, 1, \dots, N_p - 1$ . The resulting chip sequence is then differentially modulated on the time-hopped pulses, using pulse-polarities  $a_{i,j+1} = a_{i,j} d_i b_j$ ,  $j = 0, 1, \dots, N_p - 2$ , and  $a_{i+1,0} = a_{i,N_p-1} d_i b_{N_p-1}$ , see Fig. 1(a). The transmitted signal is written as

$$s(t) = \sum_{i=-\infty}^{\infty} \sum_{j=0}^{N_p-1} a_{i,j} \bar{w}(t - t_{i,j}) \quad (2)$$

where  $\bar{w}(t)$  is the transmitter pulse shape including the influence of the transmitter *and* receiver antennae. The time instants of the pulses are defined as  $t_{i,j} = iT_s + c_j$ , where  $T_s$  is the constant symbol duration and  $\{c_j\}$  are the relative pulse timings (in seconds) within a symbol, representing the time hopping code and

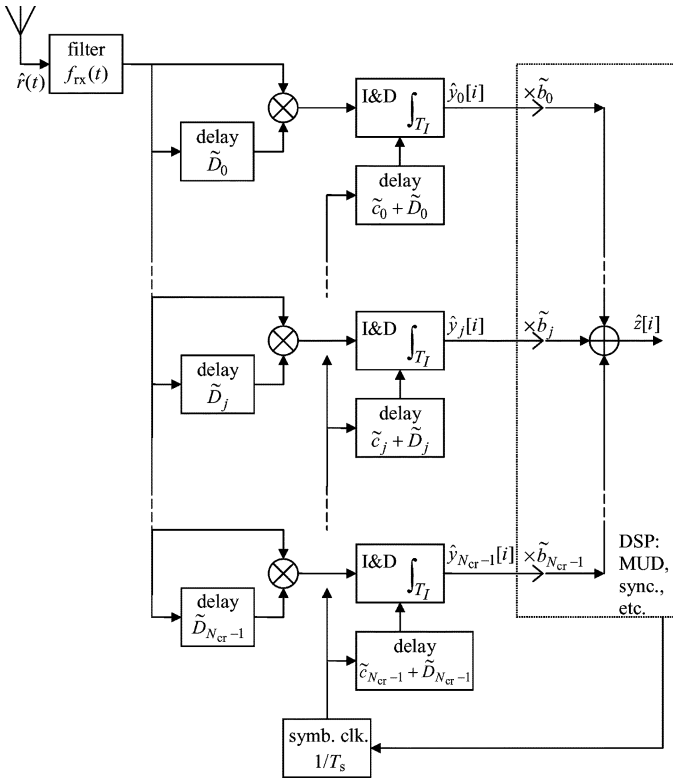


Fig. 2. Receiver front-end for a multiuser differential IR-UWB system.

the (average) spacing between pulses. Note that every second pulse of a symbol is *not* modulated by data, since  $d_i^2 = 1$ . We distinguish unmodulated reference pulses and modulated data pulses.

In this paper, we assume that the code sequences  $\{b_j\}$  and  $\{c_j\}$  do not change from symbol to symbol. This is a condition for the proposed discrete-time equivalent system model to be time-invariant. Moreover, the pulse with index  $j = 0$  must be a reference pulse.

Throughout this paper, we will study the so-called “frame-differential” IR scheme [14], which is illustrated in Fig. 1(a). Note that this scheme is a modification of the TR technique proposed in [1], where “isolated” doublets of reference and data pulses have been considered. However, by increasing the data rate these doublets move close together, thus, at a certain point, it makes sense using each pulse as a reference for demodulating the following one. Multiple access will be supported by the amplitude code  $\{b_j\}$  and by the delay hopping code  $\{D_j\}$ , defined by  $D_j = t_{i,j+1} - t_{i,j} = c_{j+1} - c_j$ ,  $j = 0, 1, \dots, N_p - 2$ , and  $D_{N_p-1} = t_{i+1,0} - t_{i,N_p-1} = T_s + c_0 - c_{N_p-1}$ .

In general, these codes and the data  $\{d_i\}$  are specific for a certain user. As the single-user case is studied in this paper, we do not indicate this dependency explicitly in order to simplify the notation.

### B. Receiver Front-End

The block diagram of a receiver front-end for such signals is shown in Fig. 2. A bank of  $N_{cr}$  pulse-pair correlators—also called AcR channels—is present at its input, comprising the delays  $\{\tilde{D}_j\}_{j=0}^{N_{cr}-1}$ , which are matched to the delay hopping code  $\{D_j\}_{j=0}^{N_p-1}$ , the multipliers, and the integrate-and-dump (I&D)

blocks. The integrators are triggered by a common symbol clock through delay elements corresponding to the pulse positions within the symbol interval. Therefore, phase-synchronization of the symbol clock is the only time-synchronization required in this receiver, assuming that the delay hopping code is known. Integration is performed over a time interval  $T_I$ , which can be selected to optimize the signal-to-noise ratio (SNR) of the AcR outputs [8], [10], [13]. In this paper, we only assume that this interval does not exceed the symbol interval  $T_I \leq T_s$ .

The outputs of the correlators are sampled at the symbol rate. The most basic receiver coherently combines these samples by canceling the amplitude code  $\{b_j\}$  through multiplication by  $\tilde{b}_j = b_j$ ,  $\forall j$ . Advanced receivers, as discussed in Section VI, can apply optimal or suboptimal detection algorithms to the combined correlator outputs, using a digital signal processor (DSP). Processing the AcR channels individually and/or fractionally-spaced sampling are other options, but both are not considered in this paper.

In order to describe the original TR scheme [1] by this model, the chip-level code can be expressed by the code sequence  $\{b_j\}_{j=0}^{N_p-1}$ . The average frame duration  $T_f$  and the delays of the pulse-pairs can be represented by  $\{c_j\}_{j=0}^{N_p-1}$ . In the receiver front-end, typically, one correlator per chip is used, thus,  $N_{cr}$  would equal the number of chips per symbol  $N_{cr} = N_p / (2N_{fpc})$ , where  $N_{fpc}$  is the number of pulse-pairs per chip.

### C. Modeling of the Receiver Front-End

Expressed mathematically, the receiver front-end performs the following operations for calculating the test statistic (decision variable) for symbol number  $i$

$$\hat{z}[i] = \sum_{j=0}^{N_{cr}-1} \hat{y}_j[i] \tilde{b}_j \quad (3)$$

$$\hat{y}_j[i] = \int_{\tilde{t}_{i,j}}^{\tilde{t}_{i,j}+T_I} \hat{r}(t) \hat{r}(t + \tilde{D}_j) dt. \quad (4)$$

In this paper, we neither consider time synchronization errors nor correlation lag offsets. That is, we assume a perfect match of the integration start times and the pulse timings  $\tilde{t}_{i,j} = t_{i,j} = iT_s + c_j$  and  $\tilde{D}_j = D_j$ . Furthermore, we choose the combining weights as  $\tilde{b}_j = b_j$ . Therefore, we will drop the tilde ( $\sim$ )—introduced above to distinguish parameters of the receiver—in the rest of this paper for simplicity. We would like to emphasize that modifying any of these assumptions would not change the structure and derivation of the equivalent system model given below.

The received signal in (4) is defined as

$$\hat{r}(t) = r(t) + \nu(t) = s(t) * h(t) * f_{rx}(t) + \bar{\nu}(t) * f_{rx}(t) \quad (5)$$

where  $r(t) = s(t) * h(t) * f_{rx}(t)$  is the received signal without noise. (The accent  $\hat{\cdot}$  is used to denote signals corrupted by additive noise.)  $\bar{\nu}(t)$  is a white Gaussian noise process,  $f_{rx}(t)$  is the impulse response of the front-end filter of our receiver, and  $*$  denotes linear convolution. The filtered noise-process  $\nu(t) = \bar{\nu}(t) * f_{rx}(t)$  is thus characterized by its autocorrelation function

$$R_\nu(\kappa) = E \{\nu(t)\nu(t + \kappa)\} = \frac{N_0}{2} f_{rx}(\kappa) * f_{rx}(-\kappa) \quad (6)$$

where  $N_0/2$  is the double-sided power spectral density of the receiver front-end noise.

The channel impulse response  $h(t)$  in (5) can be an arbitrary impulse response. It can, for instance, be modeled as a sum of Dirac delta pulses  $h(t) = \sum_n \alpha_n \delta(t - \tau_n)$  in order to express a realization of a simulated channel impulse response, generated according to the Saleh and Valenzuela channel model [17] or any of its derivatives for UWB channels [18], [19]. It can also be a measured channel impulse response. However, we assume that the time variation of the channel is slow compared with the symbol duration, for yielding a quasi-static system model.

Using the signal model (5) with (4), we obtain

$$\hat{y}_j[i] = y_j[i] + \nu_{1,j}[i] + \nu_{2,j}[i] + \nu_{3,j}[i] \quad (7)$$

$$y_j[i] = \int_{t_{i,j}}^{t_{i,j}+T_I} r(t)r(t+D_j)dt \quad (8)$$

$$\nu_{1,j}[i] = \int_{t_{i,j}}^{t_{i,j}+T_I} \nu(t)r(t+D_j)dt \quad (9)$$

$$\nu_{2,j}[i] = \int_{t_{i,j}}^{t_{i,j}+T_I} r(t)\nu(t+D_j)dt \quad (10)$$

$$\nu_{3,j}[i] = \int_{t_{i,j}}^{t_{i,j}+T_I} \nu(t)\nu(t+D_j)dt. \quad (11)$$

In order to derive the equivalent system model, we first analyze the receiver in the noise-free case (8), which will lead to a second-order Volterra system model (Section III). Subsequently, noise is analyzed in Section IV.

### III. EQUIVALENT SYSTEM MODEL WITHOUT NOISE

Using the mathematical definitions from above, the received signal can be written as

$$r(t) = \sum_{i=-\infty}^{\infty} \sum_{l=0}^{N_p-1} a_{i,l}g(t-t_{i,l}) \quad (12)$$

where  $g(t) = h(t) * w(t) = h(t) * \bar{w}(t) * f_{rx}(t)$  is the response of the channel to one transmitted monocycle at  $t = 0$ . With (8), the output of correlator  $j$  at time step  $i$  becomes

$$\begin{aligned} y_j[i] &= \int_{t_{i,j}}^{t_{i,j}+T_I} \sum_{n=-\infty}^{\infty} \sum_{l=0}^{N_p-1} a_{i+n,l}g(t-t_{i+n,l}) \\ &\quad \times \sum_{n'=-\infty}^{\infty} \sum_{l'=0}^{N_p-1} a_{i+n',l'}g(t-t_{i+n',l'}+D_j)dt \\ &= \sum_{n=-\eta}^1 \sum_{l=0}^{N_p-1} \sum_{n'=-\eta}^1 \sum_{l'=0}^{N_p-1} a_{i+n,l}a_{i+n',l'} \\ &\quad \times I_g(t_{i,j}-t_{i+n,l}, t_{i,j}-t_{i+n',l'}+T_I; \\ &\quad D_j+t_{i+n,l}-t_{i+n',l'}) \end{aligned} \quad (13)$$

where

$$I_g(t_1, t_2; \tau) = \int_{t_1}^{t_2} g(t)g(t+\tau)dt. \quad (14)$$

This integral, being a time-gated autocorrelation function of the channel response  $g(t)$ , can be evaluated numerically if measurements or simulations of  $g(t)$  are available.

Equation (13) accounts for the interference from all pulses of  $\eta$  previous and one consecutive symbol. We define the memory length  $\eta = \lceil \tau_{\max}/T_s \rceil$  and assume that the channel response  $g(t)$  is confined to the interval  $t \in [0, \tau_{\max}]$ , i.e.,  $\tau_{\max}$  is the channel's maximum excess delay. One consecutive symbol has to be considered if the integration interval  $T_I$  extends into symbol  $i+1$  and if  $T_I \leq T_s$ .

Fig. 1(b) illustrates the influence of multiple pulses on the correlation result of the demodulated pulse-pair  $l=2$  and  $l'=3$ .

In a compact matrix notation, (13) can be written as

$$y_j[i] = \mathbf{a}^T[i] \mathbf{Y}_j \mathbf{a}[i] \quad (15)$$

where

$$\mathbf{a}[i] = [a_{i-\eta,0}, a_{i-\eta,1}, \dots, a_{i+1,N_p-2}, a_{i+1,N_p-1}]^T \quad (16)$$

represents the polarities of all pulses. The elements of the  $N_p(\eta+2) \times N_p(\eta+2)$  matrix  $\mathbf{Y}_j$  are given by

$$\begin{aligned} [\mathbf{Y}_j]_{(n+\eta)N_p+l+1, (n'+\eta)N_p+l'+1} &= I_g(t_{i,j}-t_{i+n,l}, t_{i,j}-t_{i+n',l'}+T_I; D_j+t_{i+n,l}-t_{i+n',l'}) \\ &= I_g\{c_j-nT_s-c_l, c_j-nT_s-c_l+T_I; \\ &\quad D_j+(n-n')T_s+c_l-c_{l'}\} \end{aligned} \quad (17)$$

for all  $n, n' \in \{-\eta, -\eta+1, \dots, 1\}$  and  $l, l' \in \{0, 1, \dots, N_p-1\}$ .

This matrix expresses the time-hopping sequence of the transmitted signal, the receiver timing matched to this sequence (i.e., the integration intervals and correlation lags), and the channel response including any linear filtering and pulse-shaping in the analog hardware. It will be a constant valued matrix, if all these factors are time-invariant and the channel is assumed (quasi) static.

The combined decision variable defined in (3) is found as

$$z[i] = \sum_{j=0}^{N_{cr}-1} b_j \mathbf{a}^T[i] \mathbf{Y}_j \mathbf{a}[i] = \mathbf{a}^T[i] \mathbf{Z} \mathbf{a}[i] \quad (18)$$

where  $\mathbf{Z} = \sum_{j=0}^{N_{cr}-1} b_j \mathbf{Y}_j$  also includes the "tuning" of the receiver to the amplitude code  $\{b_j\}$ .

We will next demonstrate that (18) constitutes a discrete-time Volterra model of order two, having the transmitted data symbols  $\{d_i\}$  at its input. To express the data dependency, we rewrite the data (and code) dependent vector  $\mathbf{a}[i]$  in terms of the data vector  $\mathbf{d}[i] = [d_{i-\eta}, d_{i-\eta+1}, \dots, d_i, d_{i+1}]^T$

$$\mathbf{a}[i] = a_{i-\eta,0} (\bar{\mathbf{p}} + \mathbf{P} \mathbf{d}[i]) \mathbf{B} \quad (19)$$

where the amplitude code  $\{b_j\}$  of the transmitted sequence is expressed by the diagonal matrix

$$\mathbf{B} = \text{diag}[1, b_0, b_0 b_1, \dots]$$

$$[\mathbf{B}]_{n,n} = \prod_{\mu=0}^{n-2} b_{\mu \bmod N_p}, \quad n = 1, 2, \dots, N_p(\eta + 2).$$

The product  $\mathbf{P}\mathbf{d}[i]$  yields a length  $N_p(\eta + 2)$  vector containing the data bits  $\{d_{i'}\}_{i'=i-\eta}^{i+1}$  at the respective positions to modulate the pulse polarities of  $\mathbf{a}[i]$ . Therefore,  $\mathbf{P} = \mathbf{I}_{\eta+2} \otimes \mathbf{s}$  is a block-diagonal matrix of dimensions  $N_p(\eta + 2) \times (\eta + 2)$  with the length  $N_p$  selection vectors  $\mathbf{s} = [0, 1, 0, 1, \dots, 1]^T$  at its main diagonal.  $\otimes$  denotes the Kronecker product. The length  $N_p(\eta + 2)$  vector  $\bar{\mathbf{p}} = \mathbf{i}_{\eta+2} \otimes (\mathbf{i}_{N_p} - \mathbf{s})$  contains ones at the elements of  $\mathbf{a}[i]$  that are not data dependent.  $\mathbf{I}_N$  and  $\mathbf{i}_N$  denote an identity matrix of size  $N \times N$  and an all-ones vector of length  $N$ , respectively.

Using (18) and (19), a second-order Volterra model is obtained

$$z[i] = (\bar{\mathbf{p}} + \mathbf{P}\mathbf{d}[i])^T \mathbf{B}\mathbf{Z}\mathbf{B}(\bar{\mathbf{p}} + \mathbf{P}\mathbf{d}[i])$$

$$= h_0 + \mathbf{h}_1^T \mathbf{d}[i] + \mathbf{d}^T[i] \mathbf{H}_2 \mathbf{d}[i]. \quad (20)$$

The linear system coefficients are expressed by the length  $\eta + 2$  coefficient vector  $\mathbf{h}_1 = \mathbf{P}^T \mathbf{B}(\mathbf{Z} + \mathbf{Z}^T) \mathbf{B} \bar{\mathbf{p}}$ . The coefficients  $\mathbf{H}_2$  of the product terms can be represented as a triangular matrix with zero-elements on the main diagonal, by appropriately adding the upper and lower triangular parts of  $\mathbf{P}^T \mathbf{B}\mathbf{Z}\mathbf{B}\mathbf{P}$  and by including its diagonal elements in the bias term  $h_0 = \bar{\mathbf{p}}^T \mathbf{B}\mathbf{Z}\mathbf{B}\bar{\mathbf{p}} + \text{Tr}\{\mathbf{P}^T \mathbf{B}\mathbf{Z}\mathbf{B}\mathbf{P}\}$ . The latter can be done since  $d_i^2 = 1$ .

These expressions suggest that linear model components relate to the interference between (the channel's response to) unmodulated reference and modulated data pulses. Nonlinear product terms are attributed to interference between *differently modulated* pulses of any two different data symbols. They, thus, appear only if significant ISI is present.<sup>1</sup> The bias term is due to interference among fixed reference pulses (the contribution  $\bar{\mathbf{p}}^T \mathbf{B}\mathbf{Z}\mathbf{B}\bar{\mathbf{p}}$ ) plus interference between *equally* modulated data pulses (the component  $\text{Tr}\{\mathbf{P}^T \mathbf{B}\mathbf{Z}\mathbf{B}\mathbf{P}\}$ ).

In Section V-A, we will use computer simulations to demonstrate the equivalence of this system model compared with a conventional simulation of the continuous-time signals of the transmission system. But first we will reintroduce noise.

#### IV. ANALYSIS OF NOISE

For the analysis of noise, we consider the three noise terms in (7). We encounter two "linear" terms  $\nu_{1,j}[i]$  (9) and  $\nu_{2,j}[i]$  (10), which depend on the received signal  $r(t)$ , and a "product" noise term  $\nu_{3,j}[i]$  (11). This agrees with previous analyses of noise in transmitted-reference systems, see, e.g., [2], [4], and [20].

<sup>1</sup>In a multiuser (MU) equivalent system model, nonlinear terms also exist if data symbols of various users overlap. An equivalent system model can be derived for the MU-case by including the interfering users' pulse polarities in the  $\mathbf{a}[i]$ -vectors and extending the  $\mathbf{Y}_j$ -matrices with all channels' auto- and cross-correlation values for any pulse-pairs. The multiuser Volterra model comprises  $\mathbf{d}[i]$ -vectors extended by the other users' data and correspondingly extended coefficient vectors and matrices.

Following [2] and [20], we assume that all three noise components at the output of the correlators are zero-mean Gaussian noise variables, which requires that the noise process  $\nu(t)$  is zero mean, that  $R_\nu(D_j) \approx 0, \forall j$ , and that the integration-time by noise-bandwidth product  $T_I W \gg 1$ .

The noise component of the decision variable  $\hat{z}[i]$  is defined by  $z_\nu[i] = \hat{z}[i] - z[i]$ . Using (3) and (7), we obtain

$$E \{z_\nu[i] z_\nu[i + \iota]\}$$

$$= \sum_{j=0}^{N_{\text{cr}}-1} \sum_{j'=0}^{N_{\text{cr}}-1} b_j b_{j'}$$

$$\times [E \{\nu_{1,j}[i] \nu_{1,j'}[i + \iota]\} + E \{\nu_{1,j}[i] \nu_{2,j'}[i + \iota]\}$$

$$+ E \{\nu_{2,j}[i] \nu_{1,j'}[i + \iota]\} + E \{\nu_{2,j}[i] \nu_{2,j'}[i + \iota]\}$$

$$+ E \{\nu_{3,j}[i] \nu_{3,j'}[i + \iota]\}] \quad (21)$$

since  $\nu_{3,j}[i]$  is uncorrelated from  $\nu_{1,j'}[i]$  and  $\nu_{2,j'}[i], \forall j, j'$ .

In the Appendix, it is demonstrated that the data-dependent covariance of the linear noise terms can be expressed by quadratic forms

$$E \{\nu_{m,j}[i] \nu_{m',j'}[i + \iota]\} = \frac{N_0}{2} \mathbf{a}^T[i] \mathbf{V}_{\iota,j,j'}^{(\nu_m \nu_{m'})} \mathbf{a}[i] \quad (22)$$

for  $m, m' \in \{1, 2\}$ . It is zero for  $|\iota| > 1$  (see the Appendix). Similarly to (15), the data dependency is contained in the vectors  $\mathbf{a}[i]$ , while the matrices  $\mathbf{V}_{\iota,j,j'}^{(\nu_m \nu_{m'})}$  express the channel impulse response  $g(t)$ , the time-hopping code  $\{c_j\}$ , and the timing of the receiver front-end. These matrices are time-invariant (like  $\mathbf{Y}_j$ ), assuming a quasi-static channel.

The covariance of the product noise terms, which are independent of channel, code, and data, is

$$E \{\nu_{3,j}[i] \nu_{3,j'}[i + \iota]\}$$

$$= E \left\{ \int_{t_{i,j}}^{t_{i,j} + T_I} \nu(t) \nu(t + D_j) dt \right.$$

$$\left. \times \int_{t_{i+\iota,j'}}^{t_{i+\iota,j'} + T_I} \nu(t') \nu(t' + D_{j'}) dt' \right\} \quad (23)$$

$$\approx \int_{A_{\iota,j,j'}^{(1,1)}} dt \int_{-\infty}^{\infty} R_\nu(\kappa) R_\nu(\kappa + D_{j'} - D_j) d\kappa \quad (24)$$

where

$$A_{\iota,j,j'}^{(1,1)} = [c_j, c_j + T_I] \cap [c_{j'} + \iota T_s, c_{j'} + \iota T_s + T_I]$$

is the intersection of the integration intervals in (23) after subtracting  $\iota T_s$ . We have assumed in (24) that  $E\{\nu(t)\nu(t+D_j)\} \approx 0, \forall j$ . This is justified, since  $\nu(t)$  is a wideband process with bandwidth  $W \gg 1/D_j, \forall j$ .  $t + \kappa := t'$  has been substituted, causing a negligible error with the integration ranges indicated.

Note that the product noise terms of several correlators are uncorrelated with one another, provided that all differential pulse spacings are unique, i.e.,  $D_j \neq D_{j'}, \forall j \neq j'$ . (To be precise,  $R_\nu(\kappa + D_j - D_{j'}) \approx 0$  must be given over the support of

$R_\nu(\kappa)$ .) They are also uncorrelated if the integration intervals do not overlap, i.e., if  $A_{\nu,j,j'}^{(1,1)} = []$ . Then, we get

$$\begin{aligned} E \{ \nu_{3,j}[i] \nu_{3,j'}[i+l] \} &\approx \delta[l] \delta[j-j'] T_I \int_{-\infty}^{\infty} R_\nu^2(\kappa) d\kappa \\ &\approx \delta[l] \delta[j-j'] T_I \frac{N_0^2}{4} \\ &\quad \times \int_{-\infty}^{\infty} |F_{\text{rx}}(f)|^4 df \end{aligned} \quad (25)$$

where  $F_{\text{rx}}(f) = \mathcal{F}\{f_{\text{rx}}(t)\}$  is the Fourier transform of the receiver front-end filter.

#### A. Noise Model

The noise model for the decision variable can be calculated using (21)–(25). Introducing  $N_2 = N_{\text{cr}} T_I \int_{-\infty}^{\infty} |F_{\text{rx}}(f)|^4 df$ , it can be expressed by<sup>2</sup>

$$E \{ z_\nu[i] z_\nu[i+l] \} = \frac{N_0}{2} \mathbf{a}^T[i] \mathbf{W}_\nu \mathbf{a}[i] + \delta[l] \frac{N_0^2}{4} N_2$$

where

$$\mathbf{W}_\nu = \sum_{m,m'} \sum_{j,j'} b_j b_{j'} \mathbf{V}_{\nu,j,j'}^{(\nu_m, \nu_{m'})}$$

Using (19), the dependence on the data vector  $\mathbf{d}[i]$  can be written explicitly, which determines the time-variance of the noise model. Therefore, following the steps leading to (20), the time/data dependency is appropriately described by two Volterra models for  $\nu = 0, 1$ <sup>3</sup>

$$\begin{aligned} E \{ z_\nu[i] z_\nu[i+l] \} &= \frac{N_0}{2} (h_{\nu,\nu,0} + \mathbf{h}_{\nu,\nu,1}^T \mathbf{d}[i] + \mathbf{d}^T[i] \mathbf{H}_{\nu,\nu,2} \mathbf{d}[i]) \\ &\quad + \delta[l] \frac{N_0^2}{4} N_2. \end{aligned} \quad (26)$$

The coefficients of the Volterra models depend on the parameters of the transmission system and on the channel response  $g(t)$ . Note that the product noise term is proportional to the integration interval  $N_2 \propto T_I$  and to the system bandwidth expressed by  $F_{\text{rx}}(f)$ , making these parameters important for the system optimization [8], [10], [13].

#### B. Model Simplifications

From (9) and (10), it can be observed that the time-variance of the noise model is caused by variations of the received signal  $r(t)$  within the integration interval. If there is little such variation, for example, because there is little IFI and ISI so we always observe relatively undisturbed realizations of  $g(t)$ , then the data dependence will be rather weak. In these cases, the time-variance can be neglected and the average covariance of the noise

<sup>2</sup>It has been assumed that the conditions leading to (25) apply. Otherwise, (23) or (24) have to be evaluated numerically to determine the contribution of the product noise terms, which can be expressed by  $N_2[l]$  for  $|l| \leq 1$ . In general, the product noise term increases, if the conditions do not apply.

<sup>3</sup>Due to the time-variance expressed by  $\mathbf{a}[i]$ ,  $E \{ z_\nu[i] z_\nu[i+1] \} \neq E \{ z_\nu[i] z_\nu[i-1] \} = (N_0/2) \mathbf{a}^T[i] \mathbf{W}_{-1} \mathbf{a}[i] = (N_0/2) \mathbf{a}^T[i-1] \mathbf{W}_1 \mathbf{a}[i-1]$ .

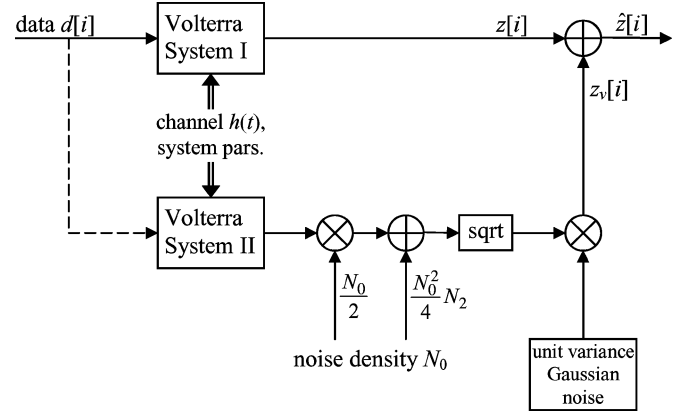


Fig. 3. Second-order Volterra equivalent system of the differential IR-UWB system. The second Volterra system models the data dependency of the noise variance at the receiver front-end's output.

samples is obtained by averaging (26) over all possible data sequences  $\mathbf{d}[i] \in \mathbb{B}^{\eta+2}$ , yielding the bias terms of the Volterra models, if the data are uncorrelated

$$E_{\mathbf{d}[i] \in \mathbb{B}^{\eta+2}} \{ E \{ z_\nu[i] z_\nu[i+l] \} \} = \frac{N_0}{2} h_{\nu,\nu,0} + \delta[l] \frac{N_0^2}{4} N_2. \quad (27)$$

In Section V-C, we will show by bit-error rate (BER) computations that even in situations of high IFI and ISI no large error is made when neglecting the noise's time-variance.

The correlation of consecutive noise samples is caused by overlapping integration intervals of any two correlators at consecutive time steps  $i$  and  $i+1$  (see the Appendix). If the system model parameters are selected such that this overlap does not occur, the covariance model can be skipped. It can also be skipped in applications where the covariance of noise is irrelevant, as for instance in the performance evaluation of a threshold detector that only considers the current decision variable  $\hat{z}[i]$  (see Section V-C).

Both, the data dependence of the variance and the covariance of noise samples become negligible when the product noise term (25) is dominant. First, this term is time-invariant and second, its samples are uncorrelated under less stringent conditions. In particular, this may apply in a critical receiver operating point at low SNR.

An illustration of the equivalent system model is shown in Fig. 3, where the upper branch with the “Volterra System I” represents the data model, while the lower branch introduces the data dependency of the noise variance, described by the “Volterra System II.” The covariance of noise samples has been omitted.

In Section V, the equivalent system model is verified by computer simulations. Unequalized performance results are computed. Our discussion concentrates on the evaluation of the significance of the various model components, like the impact of nonlinear terms and noise coloring.

## V. MODEL VALIDATION AND DISCUSSION

The following main system parameters have been used in these simulations. Average symbol duration  $T_s = 8$  ns

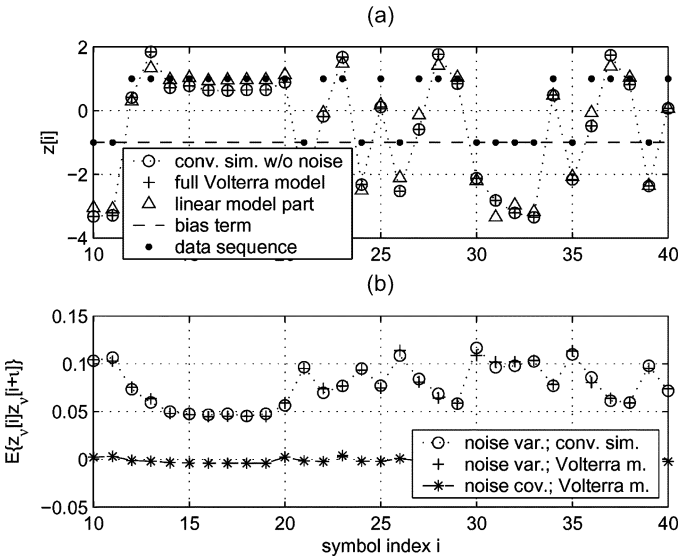


Fig. 4. Simulated receiver output compared with the output of the second-order Volterra equivalent system. (a) Noise-free case. (b) Data dependency of the noise (co)-variance at  $E_b/N_0 = 30$  dB.

(125 Mbit/s),  $N_p = 4$  pulses per symbol, integration time  $T_I = T_s = 8$  ns, a random time-hopping code of length  $N_p$  with unique interpulse delays according to the conditions for (25), i.e.,  $D_j \in \{1.7, 1.9, 2.1, 2.3\}$  ns, and a random  $\{b_j\}$ -code.

A non-line-of-sight channel has been simulated (no dominant line-of-sight component), with an exponentially decaying delay profile at RMS delay spreads [17] of  $\tau_{\text{rms}} = 5$  ns for the system validation and  $\tau_{\text{rms}} = 10$  ns for BER results [14]. The channel simulator produces random ray arrival times corresponding to a Poisson process, with a mean arrival rate of  $\lambda = 5$  rays per nanosecond. The ray-amplitudes are Rayleigh distributed with random signs.<sup>4</sup>

A second-derivative Gaussian monocycle with  $\tau_m = 0.2877$  ns has been selected for  $w(t)$ , i.e.,  $w(t) = [1 - 4\pi(t/\tau_m)^2] \exp[-2\pi(t/\tau_m)^2]$ . The continuous-time signals of the receiver were simulated by sampling at  $f_s = 20$  GHz. Higher time-resolutions (ten times) were used in the channel simulator to appropriately model the unquantized ray arrival times. Independent Gaussian noise samples were assumed at the receiver front-end, corresponding to a noise process with a bandwidth  $W = f_s/2$ .

#### A. Equivalent System Model

We first compare the receiver output  $z[i]$ , simulated by processing the received signal according to the elements of the receiver front-end shown in Fig. 2—so-called “conventional simulations”—with the output of the second-order Volterra equivalent system, whose parameters have been computed using the equations derived in Section III.

Fig. 4(a) validates the equivalence of the two simulations in the noise-free case and illustrates the impact of the nonlinear

<sup>4</sup>We do not use the standardized IEEE802.15.3a channel model in our simulations since it is not our goal to evaluate the absolute performance limits of the investigated transmission schemes and receivers. The applied model has the advantage of being fully specified by just a few well-known parameters. We expect to be able to draw the same conclusions from it, concerning the presented validation of the equivalent system model and comparison of detectors.

coefficients. The sampled output of the conventional simulation is marked by “o.” Plus characters “+” show the output of the equivalent system model at these sampling instants. Perfect agreement between these two demonstrates the suitability of the proposed equivalent system model.

More instructive is the comparison to the output of a linear system model, if the product terms of the Volterra system are neglected (see  $\Delta$ ). Clearly, this simplified model does not accurately describe the differential UWB receiver front-end. For reference, the data sequence  $\{d_i\} \in \mathbb{B}$  is shown by “.”

The horizontal dashed line stands for the bias term, which is a possible choice for the decision threshold since it represents a constant offset in the data model. But it will not be the optimal choice, because the likelihood functions of the decision variable  $\hat{z}[i]$  conditioned on the desired bit  $d_i$  are not symmetric under ISI, as seen from the product terms of the Volterra model. Specifically, if the desired  $d_i$  is fixed, the coefficients of the product terms involving  $d_i$  are either added (if  $d_i = +1$ ) or subtracted (if  $d_i = -1$ ) to the linear model coefficients, see (1) for  $m = 0$ . Furthermore, the noise variance is data dependent, as suggested by the noise model and visualized in Fig. 4(b).

Fig. 4(b) compares the variance of the additive noise  $\text{var}\{z_v[i]\}$  at the same set of observed decision variables, for a conventional simulation “o” and for the model (26) “+.” In the conventional simulation runs, one of 1000 independent noise processes has been added to the receiver front-end at a time, while using a constant data sequence and channel realization. The well matching simulation results indicate that the data-dependence of the noise variance can be very significant. The noise covariance, illustrated by asterisks “\*,” is insignificant.

A model validation by means of BER results has been given in [21].

#### B. Volterra Model Coefficients

In Fig. 5, the RMS magnitudes of the coefficients of the three Volterra models are visualized, using a gray scale corresponding to the log-magnitude (base 10). These statistics were derived from 1000 independent channel and system realizations. In Fig. 5(a), the data model is analyzed. In Fig. 5(b), the noise variance model and in Fig. 5(c), the noise covariance model. The upper triangular parts represent the coefficients of the product terms, the bottom rows stand for the linear coefficients (designated “ln”), and the first elements in the second-last rows are the bias terms (designated “bs”). Symbol index zero denotes the desired symbol.

The coefficients of the data model have been normalized by the maximum, the linear coefficient of the desired term  $h_{1,0}$ . Note that the bias term is the second largest one. Furthermore, it is evident that the major coefficients of the product terms are not much less than the linear ISI terms. Thus, significant impact of the nonlinear model components is expected under ISI.

The coefficients of both noise models have been normalized by the same value, the dominating bias term of the noise variance model [Fig. 5(b)]. This dominant bias term relates to the average variance of the additive noise samples, as noted in (27). According to this figure, the maximum data dependency will be caused by the desired data symbol, quantified through the linear coefficient at index zero. It is by a factor of about five below

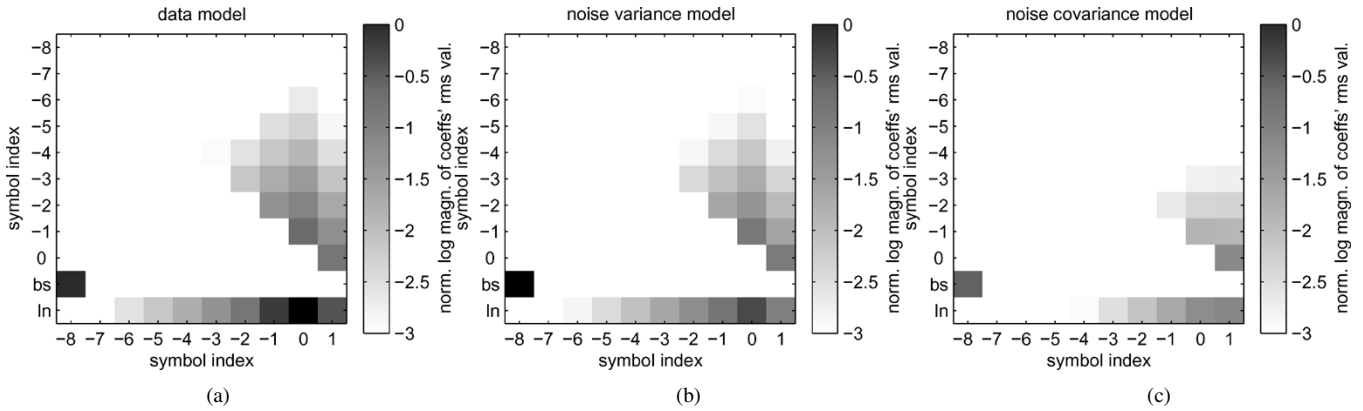


Fig. 5. Logarithm (base 10) of the normalized RMS magnitudes of the coefficients of the second-order Volterra equivalent system model. (a) Data model. (b) Noise variance model. (c) Noise covariance model.

the bias term. The noise covariance model is also dominated by the bias term [Fig. 5(c)]. It is by a factor of about ten below the bias of the noise variance model, indicating that the covariance of noise samples can be expected to be rather small. This is remarkable, since the integration ranges of consecutive samples overlap significantly in the investigated system, which was identified as the cause of noise correlation.

For clarity, these analyses have been presented for a channel with  $\tau_{\text{rms}} = 5$  ns. Increasing the RMS delay spread to a more realistic 10 ns raises the memory length to  $\eta = 15$ . But none of the above observations change and even the numeric results given remain accurate.

C. BER Results

Before introducing equalization, BER results are shown for a conventional threshold detector, which compares the decision variable  $\hat{z}[i]$  with the bias term of the data model  $h_0$

$$\hat{d}_i = \text{sign} \{ \hat{z}[i] - h_0 \}.$$

Since the variance and mean of  $\hat{z}[i]$  are known from (20) and (26), the error function can be used to compute the error probability conditioned on  $\mathbf{d}[i]$ . Averaging over all possible data sequences, the mean BER is obtained, for a given channel realization  $h(t)$ , as

$$\overline{P_e} = \frac{1}{2^{n+2}} \sum_{\mathbf{d}[i] \in \mathbb{B}^{n+2}} Q \left( \frac{(z[i] - h_0) d_i}{\sqrt{E \{ z_v^2[i] \}}} \right). \quad (28)$$

Performance results calculated with this equation are depicted in Fig. 6. For all BER simulations, the RMS delay spread has been increased to  $\tau_{\text{rms}} = 10$  ns. In order to visualize the high variability of these results for different channel realizations, we compare the mean, median, and 10% and 90% quantiles of the BERs obtained analytically for 1000 simulated channels (lines marked by “o”). These vast variations, comparable to fast fading in a narrowband system, are caused by introducing severe IFI and ISI in a TR UWB system. For comparison, the performance is also analyzed for a system

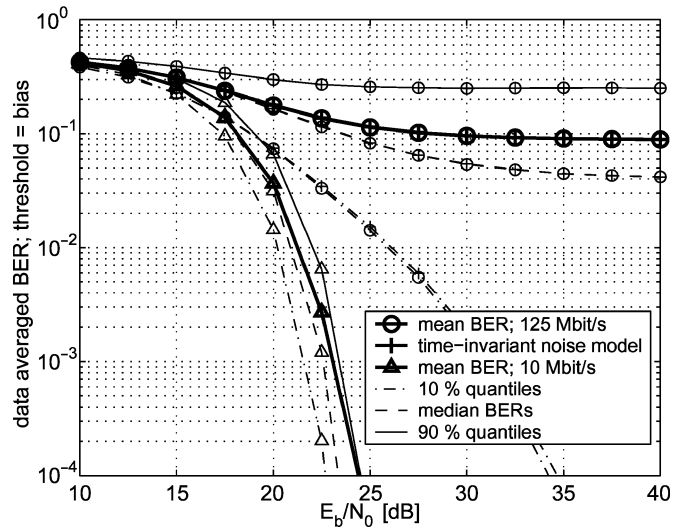


Fig. 6. Data averaged BER results for  $N = 1000$  independent channel realizations at  $\tau_{\text{rms}} = 10$  ns. Transmission scheme: “o” and “+”: 125 Mbit/s,  $T_s = 8$  ns; “ $\Delta$ ”: 10 Mbit/s,  $T_s = 100$  ns; random codes  $\{b_j\}$  and  $\{c_j\}$ ;  $N_p = 4$ ,  $T_I = 8$  ns. Evaluation of simplified noise model at 125 Mbit/s: “o”: full noise model used; “+”: fixed noise variance assumed.

suffering from very little IFI and ISI (lines marked by “ $\Delta$ ”). Its key parameters are a data rate of 10 Mbit/s ( $T_s = 100$  ns),  $N_p = 4$ ,  $D_j \in \{24.7, 24.9, 25.1, 25.3\}$  ns, and  $T_I = 8$  ns, i.e., essentially, the average pulse separation was raised to 25 ns. Under these conditions, the multipath channel is nicely resolved by the AcR front-end, evident in steeply descending and hardly varying BER curves.

In this figure, we also seek to evaluate the impact of the time-variability of the noise variance for the high-rate system. All curves indicated by “+” represent the BERs obtained if a constant noise variance is considered, as suggested in (27). Even though there is a large amount of IFI and ISI present, there is hardly any difference between the BERs for the exact model (o) and for the simplified model (+). This is a strong indication that the error made by assuming the simplified noise model is limited.

In Section VI, equalization will be applied in order to enhance the system performance and reduce its variability over multiple channel realizations.

## VI. EQUALIZATION

As indicated in the introduction, the proposed system model can be used to develop signal processing algorithms for equalization, which will be illustrated in this section.

To equalize a Volterra system, many methods have been presented in literature. In [22], a linear equalizer is proposed. However, such an equalizer requires a large spatial and/or temporal oversampling factor, which will increase the cost of the receiver considerably. Equalizing a Volterra system with a Volterra filter can avoid this problem. To design such a Volterra equalizer, we refer the interested reader to [23] and [24]. Another approach is taken in [25] and [26], where the equalization problem is viewed as a fixed point problem which is solved iteratively. In [25], the iterations are carried out on a symbol level and the previous symbols are assumed known, whereas in [26], the iterations are carried out on a sequence level and all symbols are assumed unknown. If the previous symbols are assumed known, it is also possible to derive a polynomial in the desired symbol which should be zero in the noiseless case. In the noisy case, the desired symbol can then be detected by either finding the symbol that is the closest to the root of the polynomial [27] or finding the symbol that minimizes the norm of the polynomial [28]. The latter method does not have to compute the roots of the polynomial and can be interpreted as an ML detector for the current symbol based on the current output sample with feedback of all previous symbols.

To equalize the Volterra system obtained in this paper, we first adopt a generalization of [28]. More specifically, we consider an ML sequence detector (MLSD) with decision feedback (DF), which assumes perfect knowledge of the Volterra coefficients at the receiver. The second approach taken includes estimation of the system parameters, by applying inverse modeling with an adaptive least mean squares (LMS) algorithm. For both equalizer structures, we also study the case where the equalizer only considers the linear terms to be present in the equivalent system model.

### A. Maximum-Likelihood Sequence Detection (MLSD)

In the presence of noise, the output of the combiner can be written as

$$\hat{z}[i] = h_0 + \mathbf{h}_1^T \mathbf{d}[i] + \mathbf{d}^T[i] \mathbf{H}_2 \mathbf{d}[i] + z_\nu[i]. \quad (29)$$

We have already indicated that the noise  $z_\nu[i]$  can be considered zero-mean Gaussian. For the sake of simplicity, we will also assume that  $z_\nu[i]$  is data-independent and white, which are only approximately true. However, if necessary, they can easily be incorporated in the proposed algorithm.

To detect the symbol sequence  $\{d_i\}$ , the conventional MLSD [29] applies the Viterbi algorithm to a trellis with  $2^{\eta+1}$  states. For this trellis, the branch metric from state  $\mathbf{q}_1[i] = [d_{i-\eta}, d_{i-\eta+1}, \dots, d_i]^T$  to state  $\mathbf{q}_2[i] = [d_{i-\eta+1}, d_{i-\eta+2}, \dots, d_{i+1}]^T$  is given by (see also [30] and the references therein)

$$m_{\text{mlsd}}(\mathbf{q}_1[i], \mathbf{q}_2[i]) = \|\hat{z}[i] - h_0 - \mathbf{h}_1^T \mathbf{d}[i] - \mathbf{d}^T[i] \mathbf{H}_2 \mathbf{d}[i]\|^2$$

where  $\mathbf{d}[i] = [d_{i-\eta}, d_{i-\eta+1}, \dots, d_{i+1}]^T$ .

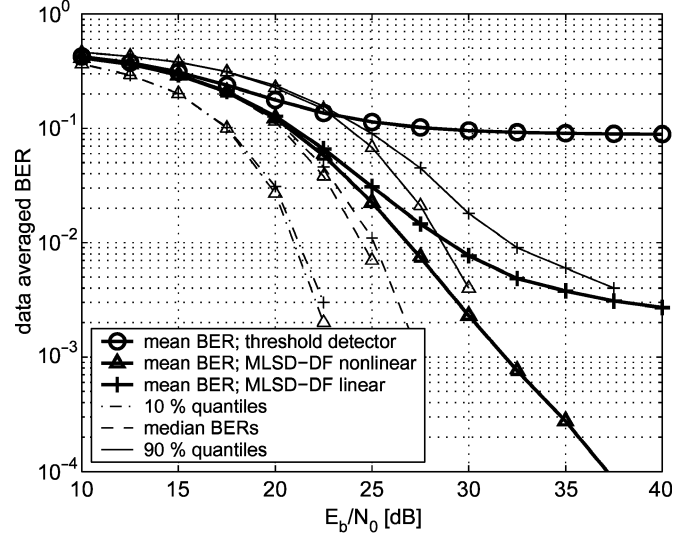


Fig. 7. BER comparison between the conventional detector and the MLSD with DF. Linear and nonlinear metric computations have been applied.

To reduce the complexity of the above MLSD, an MLSD with DF has been presented in [31]–[33]. This detector applies the Viterbi algorithm to a reduced-state trellis with only  $2^{\eta-L+1}$  states ( $1 \leq L \leq \eta$ ). For this reduced-state trellis, the branch metric from state  $\mathbf{q}_1[i] = [d_{i-\eta+L}, d_{i-\eta+L+1}, \dots, d_i]^T$  to state  $\mathbf{q}_2[i] = [d_{i-\eta+L+1}, d_{i-\eta+L+2}, \dots, d_{i+1}]^T$  is given by

$$m_{\text{mlsd-df}}(\mathbf{q}_1[i], \mathbf{q}_2[i]) = \left\| \hat{z}[i] - h_0 - \mathbf{h}_1^T \hat{\mathbf{d}}[i] - \hat{\mathbf{d}}^T[i] \mathbf{H}_2 \hat{\mathbf{d}}[i] \right\|^2$$

where  $\hat{\mathbf{d}}[i] = [\hat{d}^T(\mathbf{q}_1[i]), d_{i-\eta+L}, d_{i-\eta+L+1}, \dots, d_{i+1}]^T$ , with  $\hat{\mathbf{d}}(\mathbf{q}_1[i])$  denoting the  $L \times 1$  vector of feedback decisions, which depends on the state  $\mathbf{q}_1[i]$  and is determined by the path histories. For more details, we refer the interested reader to [31]–[33].

In Fig. 7, the performance of the conventional detector and the proposed MLSD with DF are compared. We also evaluate an MLSD-DF, where only the linear components of the Volterra system are considered in the computation of the branch metrics. For the feedback vector, we choose  $L = \eta - 1$ , leading to a trellis of only four states. The adopted parameters are the same as before, for  $\tau_{rms} = 10$  ns and 125 Mbit/s. We clearly observe that the MLSD with DF appears to be quite robust in a multipath environment. Not only the mean but also the variations of the BER results improve significantly, whereas the complexity of this receiver is still within operational limits. If the nonlinear nature of the equivalent system model is neglected (results indicated by “+”), the achieved performance is clearly worse, particularly at high SNR. Note that few ill-conditioned channel realizations seem to be responsible for the irreducible error floor and 10% worst performance results. In these cases, significant gain is obtained, when we introduce full knowledge of the nonlinear model.

Perfect knowledge of the model coefficients has been assumed in this equalization approach. Estimating the coefficients of the Volterra model is required for applying this method in a real system, which raises questions about the identifiability of the model coefficients. We will not discuss the estimation problem in this paper. To introduce a more practical detector, we introduce in the following section an adaptive equalization technique, employing a known training sequence.

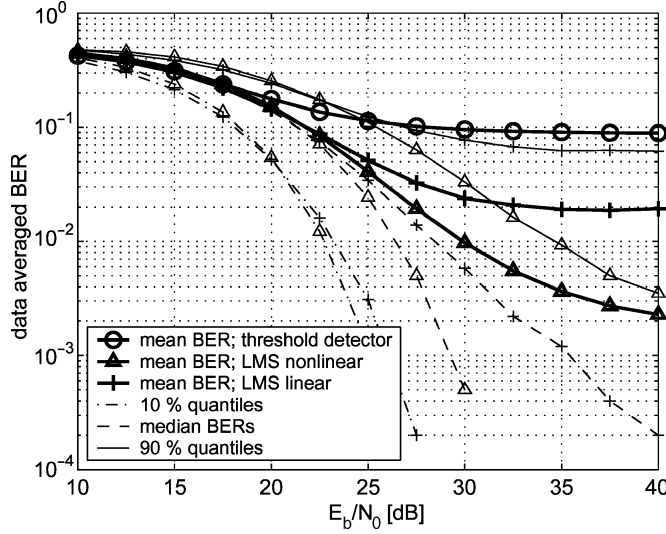


Fig. 8. BER comparison of the conventional detector with an inverse modeling approach using an adaptive LMS algorithm to adapt the coefficients of a linear (+) and a second-order Volterra ( $\Delta$ ) equalization filter.

### B. Inverse Modeling

In the inverse modeling approach, the noisy decision variable  $\hat{z}[i]$  is fed into an adaptive equalization filter denoted  $\mathbf{c}[i]$ . The output of this filter is compared with the known training sequence  $\{d_i\}$ , yielding an error signal that can be used in an adaptive LMS algorithm for updating  $\mathbf{c}[i]$  in order to minimize the error. This approach is well-known for linear equalizers and can be extended to higher order polynomial filters [34]. In the second-order case, the input tap vector consists of the decision variables and their products, written as

$$\mathbf{x}[i] = [\hat{z}[i+1], \hat{z}[i], \dots, \hat{z}[i-\eta], \hat{z}^2[i+1], \hat{z}[i+1]\hat{z}[i], \dots, \hat{z}^2[i-\eta]]^T.$$

Correspondingly, the coefficient vector is composed of linear and product coefficients

$$\mathbf{c}[i] = [c_1[i], c_0[i], \dots, c_{-\eta}[i], c_{1,1}[i], c_{1,0}[i], \dots, c_{-\eta,-\eta}[i]]^T.$$

The error signal is then computed as  $e[i] = d_i - \mathbf{c}^T[i]\mathbf{x}[i]$ , which is used in the coefficient update expressed by

$$\mathbf{c}[i+1] = \mathbf{c}[i] + \mu \mathbf{x}[i]e[i]$$

where  $\mu$  is the step size of the algorithm that can be chosen differently for the linear and nonlinear parts.

Simulation results for this algorithm are given in Fig. 8. Several hundred training symbols were used in these simulations to yield good adaptation of the equalization filter. Again, significant gains are achieved and the linear method is clearly outperformed by the nonlinear version.

## VII. CONCLUSION

A discrete-time equivalent system model has been derived for differential IR-UWB systems under severe ISI. It is applicable for a class of UWB systems in which data is differentially modulated between reference and data pulses, commonly known as

TR systems, and modified here to achieve higher efficiency by reusing each pulse as a reference, as well as a data pulse. The single-user high-data-rate case has been studied, but the model can be extended for multiuser scenarios.

It has been shown that a nonlinear second-order Volterra system appropriately models the ISI due to the multipath channel. Binary data are applied at the input of this equivalent system, resulting at its output in an accurate description of the decision variable. Nonlinear model components arise whenever pulses of different data symbols interfere with each other, i.e., in case of ISI or multiple-access interference. Exact models have been derived for the variance and covariance of the additive noise component of the decision variable. These statistical moments are data dependent and, thus, time-variant, which can be described again by second-order Volterra systems. Simplifications of the noise model have been discussed and evaluated.

The equivalent system model has been used to compute the BER performance conditioned on a channel realization. These performance results show very large variations when studied for different channel realizations, indicating that in presence of heavy ISI, an AcR can no longer resolve the multipath channel. Interference between multipath components causes BER variations similarly to fading in narrowband systems.

An accurate description of the equivalent system model is an important tool for developing optimal and suboptimal receivers based on the symbol rate output samples of the receiver front-end, the sampled decision variable. As an example, the equalization of the Volterra system is demonstrated in this paper, using an MLSD with nonlinear decision feedback and using a nonlinear inverse modeling approach based on a known training sequence and an LMS algorithm for the coefficients update. Both approaches yield significantly improved performance and reduced BER variability over multiple channels.

## APPENDIX LINEAR NOISE TERMS

We first derive the covariance of  $\nu_{1,j}[i]$  and  $\nu_{1,j'}[i+l]$ , which is determined by the system parameters, the channel response  $g(t)$ , and the data vector  $\mathbf{d}[i]$  expressed by  $\mathbf{a}[i]$ . From (9) follows with (12)

$$\begin{aligned} & E \{ \nu_{1,j}[i] \nu_{1,j'}[i+l] \} \\ &= \sum_{n=-\eta}^1 \sum_{l=0}^{N_p-1} \sum_{n'=-\eta}^1 \sum_{l'=0}^{N_p-1} a_{i+n,l} a_{i+n',l'} \\ & \quad \times \int_{t_{i,j}}^{t_{i,j}+T_I} \int_{t_{i+l,j'}}^{t_{i+l,j'}+T_I} g(t+D_j-t_{i+n,l}) g(t'+D_{j'}-t_{i+n',l'}) \\ & \quad \times E \{ \nu(t) \nu(t') \} dt' dt \end{aligned} \quad (30)$$

$$= \frac{N_0}{2} \mathbf{a}^T [i] \mathbf{V}_{\nu,j,j'}^{(\nu_1,\nu_1)} \mathbf{a}[i] \quad (31)$$

exchanging the order of summations, integrations, and the expectation.  $N_0$  is the noise power spectral density, which is written explicitly in (31), making the vector quadratic form independent of the noise power, as shown below.

Adopting the compact matrix notation, the matrix  $\mathbf{V}_{\nu,j,j'}^{(\nu_1,\nu_1)}$  expresses the channel impulse response  $g(t)$ , the time-hopping

code  $\{c_j\}$ , and the timing of the receiver front-end. It is time-invariant, assuming a quasi-static channel. Its elements are written as

$$\begin{aligned} & \left[ \mathbf{V}_{\iota, j, j'}^{(\nu_1 \nu_1)} \right]_{(n+\eta)N_p+l+1, (n'+\eta)N_p+l'+1} \\ &= \frac{2}{N_0} \int_{t_{i,j}}^{t_{i,j}+T_I} g(t+D_j-t_{i+n,l}) \\ & \quad \times \int_{t_{i+\iota, j'}-t}^{t_{i+\iota, j'}+T_I-t} g(t+\kappa+D_{j'}-t_{i+n',l'}) R_\nu(\kappa) d\kappa dt \\ & \approx \int_{A_{\iota, j, j'}^{(1,1)}} g(t+D_j-nT_s-c_l) \bar{g}(t+D_{j'}-n'T_s-c_{l'}) dt \end{aligned}$$

for all  $n, n' \in \{-\eta, -\eta+1, \dots, 1\}$  and  $l, l' \in \{0, 1, \dots, N_p-1\}$ , using the substitution  $t+\kappa := t'$  and (6). The integration interval  $A_{\iota, j, j'}^{(1,1)} = [c_j, c_j+T_I] \cap [c_{j'}+\iota T_s, c_{j'}+\iota T_s+T_I]$  is the intersection of the integration intervals in (30) and  $\bar{g}(t) = g(t) * f_{rx}(t) * f_{rx}(-t)$ .

These expressions can be evaluated numerically if the channel response  $g(t)$  is known. The approximation simplifies the evaluation. It is based on the assumption that the support of  $R_\nu(\kappa)$  is very short compared with the integration interval  $T_I$ , due to the large signal bandwidth.

Following similar steps, we obtain  $E\{\nu_{m,j}[\iota] \nu_{m',j'}[\iota+\iota]\} = (N_0/2) \mathbf{a}^T[\iota] \mathbf{V}_{\iota, j, j'}^{(\nu_m \nu_{m'})} \mathbf{a}[\iota]$ , for  $m, m' \in \{1, 2\}$ , where

$$\begin{aligned} & \left[ \mathbf{V}_{\iota, j, j'}^{(\nu_1 \nu_2)} \right]_{(n+\eta)N_p+l+1, (n'+\eta)N_p+l'+1} \\ & \approx \int_{A_{\iota, j, j'}^{(1,2)}} g(t+D_j-nT_s-c_l) \bar{g}(t-D_{j'}-n'T_s-c_{l'}) dt \\ & \left[ \mathbf{V}_{\iota, j, j'}^{(\nu_2 \nu_1)} \right]_{(n+\eta)N_p+l+1, (n'+\eta)N_p+l'+1} \\ & \approx \int_{A_{\iota, j, j'}^{(2,1)}} g(t-D_j-nT_s-c_l) \bar{g}(t+D_{j'}-n'T_s-c_{l'}) dt \\ & \left[ \mathbf{V}_{\iota, j, j'}^{(\nu_2 \nu_2)} \right]_{(n+\eta)N_p+l+1, (n'+\eta)N_p+l'+1} \\ & \approx \int_{A_{\iota, j, j'}^{(2,2)}} g(t-D_j-nT_s-c_l) \bar{g}(t-D_{j'}-n'T_s-c_{l'}) dt \end{aligned}$$

for all  $n, n' \in \{-\eta, -\eta+1, \dots, 1\}$  and  $l, l' \in \{0, 1, \dots, N_p-1\}$ , with

$$\begin{aligned} A_{\iota, j, j'}^{(1,2)} &= [c_j, c_j+T_I] \\ & \quad \cap [c_{j'}+D_{j'}+\iota T_s, c_{j'}+D_{j'}+\iota T_s+T_I] \\ A_{\iota, j, j'}^{(2,1)} &= [c_j+D_j, c_j+D_j+T_I] \\ & \quad \cap [c_{j'}+\iota T_s, c_{j'}+\iota T_s+T_I] \\ A_{\iota, j, j'}^{(2,2)} &= [c_j+D_j, c_j+D_j+T_I] \\ & \quad \cap [c_{j'}+D_{j'}+\iota T_s, c_{j'}+D_{j'}+\iota T_s+T_I]. \end{aligned}$$

From the integration intervals  $\{A_{\iota, j, j'}^{(m, m')}\}_{m, m' \in \{1, 2\}}$  follows that  $E\{\nu_{m,j}[\iota] \nu_{m',j'}[\iota+\iota]\} = 0$  for  $|\iota| > 1$ , under the conditions that  $T_I \leq T_s$  and  $c_j \in [0, T_s - D_j], \forall j$ , which are fulfilled in practical transmitted-reference UWB systems.

## REFERENCES

- [1] R. Hocht and H. Tomlinson, "Delay-hopped transmitted-reference RF communications," in *IEEE Conf. Ultra Wideband Syst. Technol.*, Baltimore, MD, May 2002, pp. 265–270.
- [2] J. Choi and W. Stark, "Performance of ultra-wideband communications with suboptimal receivers in multipath channels," *IEEE J. Sel. Areas Commun.*, vol. 20, no. 9, pp. 1754–1766, Dec. 2002.
- [3] M. Ho, V. S. Somayazulu, J. Foerster, and S. Roy, "A differential detector for an ultra-wideband communications system," in *IEEE Veh. Technol. Conf.*, Spring 2002, pp. 1896–1900.
- [4] A. Trindade, Q. Dang, and A.-J. van der Veen, "Signal processing model for a transmit-reference UWB wireless communication system," in *Proc. IEEE Conf. Ultra-Wideband Syst. Technol.*, Reston, VA, Nov. 2003, pp. 270–274.
- [5] H. Zhang and D. Goeckel, "Generalized transmit-reference UWB systems," in *Proc. IEEE Conf. Ultra-Wideband Syst. Technol.*, Reston, VA, Nov. 2003, pp. 147–151.
- [6] Y.-L. Chao and R. A. Scholtz, "Optimal and suboptimal receivers for ultra-wideband transmitted reference systems," in *Proc. IEEE Global Telecommun. Conf.*, San Francisco, CA, Dec. 2003, pp. 759–763.
- [7] S. Franz and U. Mitra, "On optimal data detection for UWB transmitted reference systems," in *Proc. IEEE Global Telecommun. Conf.*, San Francisco, CA, Dec. 2003, pp. 744–748.
- [8] —, "Integration interval optimization and performance analysis for UWB transmitted reference systems," in *Proc. Int. Workshop UWB Syst. Joint Conf. UWB Syst. Technol., Joint UWBS and IWUWBS*, Kyoto, Japan, May 2004, pp. 26–30.
- [9] L. Yang and G. Giannakis, "Optimal pilot waveform assisted modulation for ultra-wideband communications," *IEEE Trans. Wireless Commun.*, vol. 3, no. 4, pp. 1236–1249, Jul. 2004.
- [10] T. Zasowski, F. Althaus, and A. Wittneben, "An energy efficient transmitted-reference scheme for ultra-wideband communications," in *Proc. Int. Workshop UWB Syst. Joint Conf. UWB Syst. Technol., Joint UWBS and IWUWBS*, Kyoto, Japan, May 2004, pp. 146–150.
- [11] G. Leus and A.-J. van der Veen, "Noise suppression in UWB transmitted reference systems," *Proc. IEEE Signal Process. Workshop Signal Process. Adv. Wireless Commun.*, pp. 155–159, Jul. 2004.
- [12] J. Romme and G. Durisi, "Transmit reference impulse radio systems using weighted correlation," in *Proc. Int. Workshop UWB Syst. Joint Conf. UWB Syst. Technol., Joint UWBS and IWUWBS*, Kyoto, Japan, May 2004, pp. 141–145.
- [13] J. Romme and K. Witrisal, "Oversampled weighted autocorrelation receivers for transmitted-reference UWB systems," in *Proc. IEEE Veh. Technol. Conf.*, Stockholm, Sweden, May 2005.
- [14] K. Witrisal, M. Pausini, and A. Trindade, "Multiuser interference and interframe interference in UWB transmitted reference systems," in *Proc. Int. Workshop UWB Syst. Joint Conf. UWB Syst. Technol., Joint UWBS and IWUWBS*, Kyoto, May 2004, pp. 96–100.
- [15] V. J. Mathews and G. L. Sicuranza, *Polynomial Signal Processing*. New York: Wiley, 2000.
- [16] M. Pausini, G. J. M. Janssen, and K. Witrisal, "Delay hopping and chip codes design for frame differential autocorrelation receiver in IR UWB systems," in *Proc. IEEE Int. Conf. Commun.*, Seoul, Korea, May 2005.
- [17] A. M. Saleh and R. A. Valenzuela, "A statistical model for indoor multipath propagation," *IEEE J. Sel. Areas Commun.*, vol. 5, no. 2, pp. 128–137, Feb. 1987.
- [18] J. Foerster and Q. Li, "UWB Channel Modeling Contribution from Intel," IEEE P802.15 Wireless Personal Area Networks Std. IEEE P802.15-02/279r0-SG3a, Jun. 2002.
- [19] J. Kunisch and J. Pamp, "An ultra-wideband space-variant multipath indoor radio channel model," in *Proc. IEEE Conf. Ultra-Wideband Syst. Technol.*, Reston, VA, Nov. 2003, pp. 290–294.
- [20] M. Pausini and G. J. M. Janssen, "Analysis and comparison of autocorrelation receivers for IR-UWB signals based on differential detection," in *Proc. Int. Conf. Acoust., Speech, Signal Process.*, Montreal, Canada, May 2004, pp. iv-513–iv-516.
- [21] K. Witrisal and M. Pausini, "Equivalent system model of intersymbol interference in a frame-differential IR-UWB receiver," in *Proc. IEEE Global Telecommun. Conf.*, Dallas, TX, Dec. 2004, pp. 3505–3510.

- [22] G. B. Giannakis and E. Serpedin, "Linear multichannel blind equalizers of nonlinear FIR Volterra channels," *IEEE Trans. Signal Process.*, vol. 45, no. 1, pp. 67–81, Jan. 1997.
- [23] M. Schetzen, "Theory of  $p$ th-order inverses of nonlinear systems," *IEEE Trans. Circuits Syst.*, vol. 23, no. 5, pp. 285–291, May 1976.
- [24] S. Benedetto and E. Biglieri, "Nonlinear equalization of digital satellite channels," *IEEE J. Sel. Areas Commun.*, vol. 1, no. 1, pp. 57–62, Jan. 1983.
- [25] C.-H. Tseng and E. J. Powers, "Nonlinear channel equalization in digital satellite systems," in *Proc. IEEE Global Telecommun. Conf.*, Houston, TX, Dec. 1993, pp. 1639–1643.
- [26] R. D. Nowak and B. D. Van Veen, "Volterra filter equalization: A fixed point approach," *IEEE Trans. Signal Process.*, vol. 45, no. 2, pp. 377–388, Feb. 1997.
- [27] A. J. Redfern and G. T. Zhou, "A root method for Volterra system equalization," *IEEE Signal Process. Lett.*, vol. 5, no. 11, pp. 285–288, Nov. 1998.
- [28] —, "Decision feedback equalization for Volterra systems—A root method," in *Proc. Asilomar Conf. Signals, Syst., Comput.*, Pacific Grove, CA, Nov. 1998, pp. 47–51.
- [29] G. D. Forney, Jr., "Maximum-likelihood sequence estimation of digital sequences in the presence of intersymbol interference," *IEEE Trans. Inf. Theory*, vol. 18, no. 3, pp. 363–378, May 1972.
- [30] A. Vannucci and R. Raheli, "Sequence detection in nonlinear channels: A convenient alternative to analog predistortion," *IEEE Trans. Commun.*, vol. 50, no. 9, pp. 1515–1524, Sep. 2002.
- [31] M. V. Eyuboğlu and S. U. H. Qureshi, "Reduced-state sequence estimation with set partitioning and decision feedback," *IEEE Trans. Commun.*, vol. 36, no. 1, pp. 13–20, Jan. 1988.
- [32] P. Chevillat and E. Eleftherious, "Decoding of trellis-encoded signals in the presence of intersymbol interference and noise," in *Proc. IEEE Int. Conf. Commun.*, Philadelphia, PA, Jun. 1988, pp. 694–699.
- [33] A. Duel-Hallen and C. Heegard, "Delayed decision-feedback sequence estimation," *IEEE Trans. Commun.*, vol. 37, no. 5, pp. 428–436, May 1989.
- [34] V. J. Mathews, "Adaptive polynomial filters," *IEEE Signal Process. Mag.*, vol. 8, pp. 10–26, Jul. 1991.



**Klaus Witrissal** (S'98–M'03) was born in Graz, Austria, in 1972. He received the Dipl.-Ing. degree in electrical engineering from Graz University of Technology, Graz, Austria, in 1997 and the Ph.D. degree (*cum laude*) from Delft University of Technology, Delft, The Netherlands, in 2002.

He was appointed as a Research Engineer at Delft University of Technology from 1997 to 2001, working on frequency-domain channel characterization and OFDM transmission technology. From January to October 2002, he was a Project

Leader with AVL, Graz. Currently, he is an Assistant Professor at the Signal Processing and Speech Communication Laboratory (SPSC), Graz University of Technology, where he runs a number of research projects in the area of ultra-wideband (UWB) communications, in cooperation with national and international partners. His research interests are in signal processing for broadband and UWB wireless communications, propagation channel modeling, and positioning.



**Geert Leus** (M'01) was born in Leuven, Belgium, in 1973. He received the Electrical Engineering degree and the Ph.D. degree in applied sciences from the Katholieke Universiteit, Leuven, Belgium, in June 1996 and May 2000, respectively.

He was a Research Assistant and a Postdoctoral Fellow of the Fund for Scientific Research, Flanders, Belgium, from October 1996 to September 2003. During that period, he was affiliated with the Electrical Engineering Department, Katholieke Universiteit Leuven, Leuven, Belgium. Currently, he

is an Assistant Professor at the Faculty of Electrical Engineering, Mathematics and Computer Science, Delft University of Technology, Delft, The Netherlands. During the summer of 1998, he visited Stanford University, and from March 2001 to May 2002, he was a Visiting Researcher and Lecturer at the University of Minnesota, Minneapolis. His research interests are in the area of signal processing for communications.

Dr. Leus received a 2002 IEEE Signal Processing Society Young Author Best Paper Award. He is a member of the IEEE Signal Processing for Communications Technical Committee. He is an Associate Editor for the IEEE TRANSACTIONS ON WIRELESS COMMUNICATIONS, the IEEE SIGNAL PROCESSING LETTERS, and the *EURASIP Journal on Applied Signal Processing*.



**Marco Pausini** (S'03) received the Dr.-Ing. degree in telecommunication engineering from the University of Bologna, Bologna, Italy, in 2001. He is currently working towards the Ph.D. degree at the Department of Electrical Engineering, Technical University of Delft, Delft, The Netherlands.

From June 2001 to June 2002, he was with CEFRIEL-ICT, Center of Excellence For Research, Innovation, Education, and Industrial Laboratories Partnership, Politecnico di Milano, Italy. His research interests include communication theory,

ultrawide bandwidth (UWB) communications systems, and smart antennas.



**Christoph Krall** (S'04) was born in St. Veit a/d Glan, Austria, in 1979. He received the Dipl. Ing. degree in electrical engineering and telecommunication engineering from Graz University of Technology, Graz, Austria, in 2005. Currently, he is working towards the Ph.D. degree as a Research Assistant at the Signal Processing and Speech Communication Laboratory, Graz University of Technology.

His research interests include wireless broadband communications, channel modeling, transceiver design, and nonlinear signal processing.